THE JOURNAL OF PHYSICAL CHEMISTRY C

Article

New Insights into the Chemistry of Thiolate-Protected Palladium Nanoparticles

Gastón Corthey, Aldo A. Rubert, Andrea Lorena Picone, Gilberto Casillas, Lisandro J. Giovanetti, Jose M. Ramallo-Lopez, Eugenia Zelaya, Guillermo A. Benitez, Felix G Requejo, Miguel Jose-Yacaman, Roberto C. Salvarezza, and Mariano Hernán Fonticelli

J. Phys. Chem. C, **Just Accepted Manuscript** • DOI: 10.1021/jp301531n • Publication Date (Web): 05 Apr 2012

New Insights into the Chemistry of Thiolate-Protected Palladium Nanoparticles

Gastón Corthey[†], *Aldo A. Rubert*[†], *A. Lorena Picone*[†], *Gilberto Casillas*[§], *Lisandro J. Giovanetti*[†], *José M. Ramallo-López*[†], *Eugenia Zelaya*[+], *Guillermo A. Benitez*[†], *Félix G. Requejo*[†], *Miguel José-Yacamán*[§], *Roberto C. Salvarezza*[†] *and Mariano H. Fonticelli*[†,*]

[†]The Research Institute of Theoretical and Applied Physical Chemistry (INIFTA), National University of La Plata - National Scientific and Technical Research Council (CONICET), Sucursal 4 Casilla de Correo 16, 1900 La Plata, Argentina.

[§]Department of Physics and Astronomy, University of Texas at San Antonio, One UTSA Circle, San Antonio, TX 78249, USA.

[+]Bariloche Atomic Center, National Atomic Energy Commission - CONICET, 8400 S. C. de Bariloche, Río Negro, Argentina.

RECEIVED DATE

*Corresponding Author

Fax: +54 221 425 4642

Phone: +54 221 425 7430

E-mail: mfonti@inifta.unlp.edu.ar,

Homepage: http://nano.quimica.unlp.edu.ar

ABSTRACT: This paper establishes the chemical nature of Pd nanoparticles protected by alkanethiolates that were prepared through a ligand place-exchange approach and the two-phase method, firstly developed for Au nanoparticles by Brust and Schiffrin. After ten years since the first study on this kind of Pd nanoparticles was published, the surface composition of the particles is a matter of debate in the literature and it has not been unambiguously assessed. The nanoparticles were studied by means of several techniques: UV-visible spectroscopy, scanning transmission electron microscopy (STEM), Fourier-transform infrared spectroscopy (FTIR), extended X-ray absorption fine structure (EXAFS) and X-ray photoelectron spectroscopy (XPS). The experimental data, obtained for the 3 nm diameter Pd particles, prepared by both synthetic routes, are consistent with nanoparticles composed by Pd(0) cores surrounded by a submonolayer of sulfide species, which are protected by alkanethiolates. Also, we unambiguously demonstrate that the chemical nature of these particles is very similar to that experimentally found for alkanethiolate-modified bulk Pd. The results from this paper are important not only for handling thiolate-protected Pd nanoparticles in catalysis and sensing, but also for the basic comprehension of metallic nanoparticles and the relation of their surface structure whit the synthesis method.

KEYWORDS: thiols, alkanethiols, amines, palladium sulfide, self-assembled monolayers

1. INTRODUCTION

Noble metal nanoparticles (NPs) have recently attracted much attention due to their unique optical, electronic, and catalytic properties. The outstanding behavior of the different kind of particles arises from their distinctive electronic properties, which are intimately related to their size and the chemical nature of their core and surface species. Among NPs of noble metals, those made of Au cores protected by thiolates represent the most studied and better understood systems. Up to the point that, also when considering other metals, is mandatory to refer to alkanethiolate-protected Au NPs. This fact resulted in some drawbacks in the comprehension upon the behavior of NPs of platinum group metals, as they behave differently than the Au ones in many aspects. This is particularly true regarding the surface chemistry of thiols on Pd.[1] It is generally accepted that thiols form a thiolate bond when they are self-assembled on Au surfaces.[2–6] On the other hand, Pd planar surfaces are better described considering a thin PdS_x surface, which is located between the bulk metal and an alkanethiolate self-assembled monolayer (SAM).[1,7] Although this structure was proposed years ago by the Whitesides' group –and later studied in more detail in our laboratory–,[1,8] the complexity of thiol/Pd system is still being underestimated. Certainly, even today it is simply described as a $\sqrt{3}\times\sqrt{3}$ R30° *n*-alkanethiolate SAM on Pd(111) surfaces.[9–11] Also, when considering the surface of Pd NPs, the same lack of precision or incomplete description of their chemistry is observed in the literature.[10,12–14] Recently, Pd particles (3.0 nm in size) prepared by the two-phase Brust-Schiffrin method[3] in the presence of hexanethiol, –for the application in hydrogen sensing and catalysis– where simply described as hexanethiolate-coated Pd monolayer-protected clusters.[12] It was assumed that the replacement of amines by thiols is dominated by the strongest Pd–SR bond, without taking into account the possibility of the formation of a sulfide layer. On the other hand, Pd NPs have been alternatively described as palladium sulfide NPs[15] or as a metallic Pd core capped by a dialkyldisulfide layer.[16] The above examples indicate a clear need for a deeper comprehension of the interface formed when Pd NPs are protected by thiol-derived species.

Regarding the applications of these kinds of particles in catalysis, very recently, Pd NPs protected by several thiols were synthesized through a one-phase approach. Although intriguing differences in the crystallinity of the particles prepared at low and room temperature were reported, no further interpretation on the chemical bases was provided.[17] They also emphasized that Suzuki cross-coupling reactions are generally carried out using relatively large amounts of expensive Pd salts or organo-palladium complexes, and Pd NPs can be used to overcome this problem. Moreover, they successfully applied 11-mercaptoundecanoic acid-covered Pd NPs as catalysts for coupling reactions, and reused this material several times. In a recent paper, it was demonstrated that thiolate-protected Pd NPs are excellent catalyst for Heck reactions.[18] In another interesting report, it was shown that alkanethiol coatings improve the selectivity of 1-epoxybutane formation from 1-epoxy-3-butene on Pd catalysts from 11 to 94% at equivalent reaction conditions and conversions. It was found that, although sulfur species are generally considered to be indiscriminate catalyst poisons, the reaction rate for the desired product on a catalyst coated with a thiol was only slightly lower than that on an uncoated catalyst. However, the thiol/Pd surface was simply described as equivalent to Au modified by thiols.[10]

All in all, proved the importance of Pd NPs due to their exceptional catalytic, sensing and magnetic[19] properties, an accurate interpretation of their electronic structure with the aim to understand the behavior of these NPs has as a prerequisite a correct description of the chemical composition and surface structure of these systems. In this regard, it is remarkable the approach made by Kornberg's and Häkkinen's groups, who precisely determined the structure of thiolate-protected Au NPs,[5] and based on it described their electronic structure.[20]

The objective of the present study is to gain insight into the composition, geometric and electronic structures of Pd NPs protected by alkanethiols, which are approximately 3 nm in size. We have compared the chemical nature of the thiol capping molecules on Pd NPs prepared by two different approaches: the NPs produced by the two-phase Brust-Schiffrin method and the ones obtained by ligand place-exchange of alkylamines by alkanethiols on previously synthesized alkylamine-protected Pd NPs.

The results were contrasted with those obtained for alkanethiolate monolayer-protected Au NPs of comparable size and also with SAMs of alkanethiolates on extended planar Pd and Au surfaces. In this paper we demonstrate that the structure and composition of thiolate-protected Pd NPs is comparable to that found for extended surfaces. Metallic Pd cores are surrounded by a palladium sulfide with submonolayer coverage, while thiolate moieties protect them from sintering. This structure is found both, for Pd NPs prepared by Brust-Schiffrin method and those produced by ligand place-exchange.

2. EXPERIMENTAL SECTION

2.1. Synthesis of the Nanoparticles. Dodecanethiolate-protected Pd NPs were synthesized by the Brust-Shriffrin method[3] or by ligand place-exchange of dodecylamine-protected Pd NPs, prepared by the Leff method.[21] Details on the synthesis of the nanoparticles are given in the Supporting Information.

2.2. UV/Visible Absorption Spectroscopy (UV/vis). UV/vis spectra were recorded with a Perkin Elmer Lambda 35 Spectrometer, equipped with a double beam. Hexane or toluene was used as reference.

2.3. Fourier-Transform Infrared Spectroscopy (FTIR). FTIR spectra were recorded on a nitrogen-purged Varian 660 spectrometer equipped with a DTGS detector. A thick film of the sample was prepared on a KBr window by drop-casting a toluene solution of the NPs, which was further dried under nitrogen. The spectra were acquired in the transmission mode with a spectral resolution of 4 cm^{-1} accumulating 128 scans. Additionally, the baselines of the spectra were corrected using the Varian FTIR spectrometer software.

2.4. Scanning Transmission Electron Microscopy (STEM). STEM was carried out with a JEOL JEM-ARM200F aberration-corrected microscope, operating at 200 kV, equipped with a Schottky FEG, a hexapole spherical aberration (C_s) probe corrector (CEOS GmbH) and a high-angle annular dark field (HAADF) detector. The probe size used for acquiring the HAADF images was 0.095 nm. The alignment of the microscope was verified through the CESCOR software. A focus/tilt tableau was acquired

measuring defocus and two-fold astigmatism as a function of both radial and azimuthal tilt angles. HAADF-STEM images were acquired with a camera length of 120 mm and a collection angle of 33-125 mrad. Nanoparticle suspension was drop-cast on an amorphous carbon covered copper grid. Details on the size distribution of the particles are included in the Supporting Information.

2.5. Extended X-Ray Absorption Fine Structure (EXAFS). EXAFS experiments at the Pd K edge (24350 eV) were performed using a RIGAKU R-XAS Looper in-house spectrometer in transmission mode. Ionization chambers filled with Xe were used to measure the incident radiation and a solid state detector to measure the transmitted intensity. Homogeneous dry samples of Pd@SC12 NPs were mounted on an acrylic sample holder. The thickness of the sample provided an X-ray absorption jump at the Pd K edge of approximately 0.75. The energy calibration and the determination of the $S_0 = 0.56 \pm 0.02$ were done using a metallic Pd foil.

2.6. X-Ray Photoelectron Spectroscopy (XPS). The samples were characterized by XPS using both a conventional X-ray source and synchrotron radiation. In the laboratory, a Mg Kα source (XR50, Specs GmbH) and a hemispherical electron energy analyzer (PHOIBOS 100, Specs GmbH) were used. A two-point calibration of the energy scale was performed using sputtered cleaned Au (Au $4f_{7/2}$, binding energy (BE) = 84.00 eV) and copper (Cu $2p_{3/2}$, BE = 932.67 eV) samples. The base pressure inside the ultra-high vacuum (UHV) camber was below 10^{-9} mbar. XPS was also performed at the SGM beamline of the Laboratorio Nacional do Luz Síncrotron (LNLS), Campinas, Brazil. This beamline is equipped with a Spherical Grating Monochromator, which allows working in the range of 250 - 1000 eV. The endstation is composed by an UHV chamber (base pressure = 10^{-8} mbar) with a hemispherical electron energy analyzer (PHOIBOS 150, Specs GmbH). The energy of the incident photons was set to 250 eV. For spectra deconvolution of the S 2*p* region, a Shirley type background and a Gaussian-Lorentzian function were used. The full width at half maximum (fwhm) was fixed at 1.1 eV in the case of 1253.6 eV of incident energy and 0.8-0.9 eV for 250 eV. The spin-orbit doublet separation of S 2*p* signal was set to 1.2 eV. The BEs and peak areas were optimized to achieve the best fit. S:Pd and C:S atomic ratios were

estimated by the measurement of the areas of Pd 3*d*, S 2*p* and C 1*s* signals, corrected by the atomic ionization cross sections at the corresponding X-ray energies.[22] The dried NPs were suspended in hexane and drop-cast on graphite or a platinum foil substrate and then dried before their introduction at the main chamber. Valence-band region was measured only in samples deposited on graphite, and C:S atomic ratio in samples deposited on platinum foil.

3. RESULTS AND DISCUSSION

The first route employed for the synthesis of dodecanethiolate-protected Pd NPs was the two-phase method developed by Brust and Schiffrin for the synthesis of thiolate monolayer-protected Au NPs.[3] This method was used for the first time with Pd by Chen, *et al.*[23] and it was later studied in more detail by Zamborini, *et al.*[24] As represented in the scheme of Figure 1, Pd(II) species that form halide complexes ($[PdCl_4]^{2-}$) are transferred from the aqueous solution to the organic phase by a quaternary ammonium salt (NR_4X). Metal ions might reside inside inverse micelles of the ammonium salt in the organic solvent.[25] As bromide anions can be exchanged with chlorides in the coordination sphere of Pd(II), the Pd complexes in the organic phase are simply called $[PdX_4]^{2-}$. Contrary to what happens when this protocol is carried out for the synthesis of Au NPs,[26] the addition of thiols (RSH) do not drive the reduction of the metallic species, *i.e.* palladium remains as Pd(II) after thiol addition. Furthermore, while recent experimental data have shown that ion-pairs of tetraalkylammonium and Au(I)-halide complexes ($[NR_4][AuX_2]$) are the real precursors in the two-phase method for the synthesis of Au NPs,[26] Pd(II)-thiol complexes are formed when thiols are added to Pd(II) species dissolved in toluene.[24] However, as the thiol amount used in the present study (0.5:1 thiol:Pd molar ratio) is lower than that needed to completely form the Pd(II)-thiolate complexes, also $[PdX_4]^{2-}$ species are present in the organic phase when the reducing agent, sodium borohydride, is added (see Supporting Information). When this happens, the reduction of Pd(II) species to Pd(0) is produced and dodecanethiolate-protected Pd NPs (Pd@SC12) are obtained. The attempts to form Pd NPs starting with thiol:Pd molar ratios higher than

1:1 have failed (see Supporting Information).[24,27] The UV-vis absorption spectroscopy data (Figure 1) correlate very well with those previously reported for Pd NPs.[13,23,24] The absence of peaks in the 300-500 nm domain, which are related to Pd(II)-thiolates,[24,27,28] indicates that no significant amount of these species is present in Pd NPs.[13,23,24] It was not possible to prepare propanethiolate-protected Pd nanoparticles because of the short hydrocarbon chain length of the thiols.

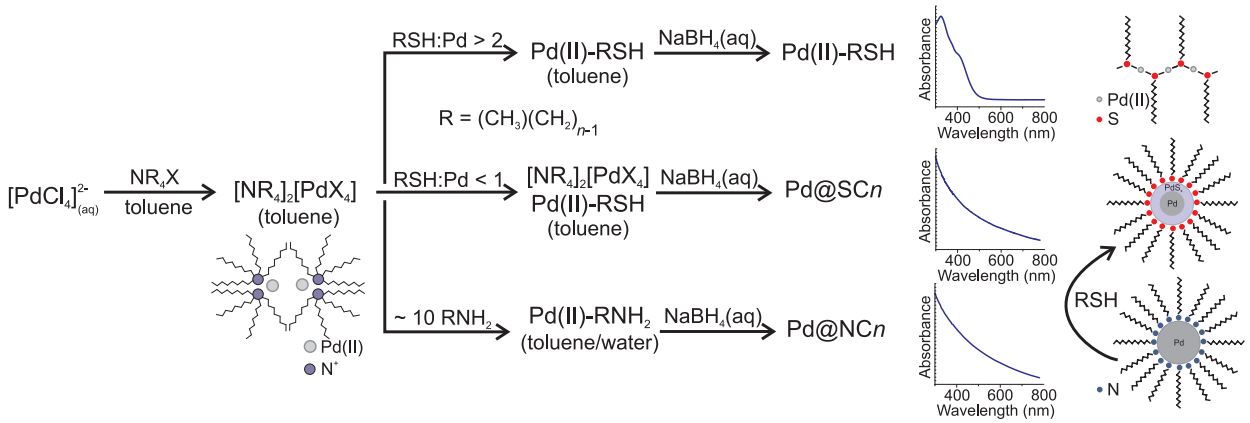

Figure 1. Scheme of the different routes for the synthesis of Pd NPs and Pd(II) thiolate complexes. The UV-vis absorption spectra of different products are also shown. For the systems studied in this paper, SC*n* = SC12 and NC*n* = NC12. The drawings are only schematic representations of the products or intermediates.

The second route employed was the ligand place-exchange of alkylamines (RNH_2) by alkanethiols on previously synthesized dodecylamine-protected Pd NPs (Pd@NC12). To prepare these particles, the Leff method was followed.[21] These particles are commonly described as a Pd(0) core protected by alkylamine molecules,[12,29] as depicted in Figure 1. However, since the interaction of alkylamines with Pd, is not as strong as with thiols, these NPs are more susceptible than Pd@SC12 ones of being oxidized by the oxygen presents in the reaction media. Therefore, some amount of palladium oxide could be present in these particles.

After rinsing Pd@NC12 NPs, they were placed in contact with dodecanethiol (thiol:Pd molar ratio ~ 1:1) in toluene overnight to accomplish the ligand place-exchange. After rinsing these particles with ethanol, Pd NPs covered by a mixture of dodecylamine and dodecanethiol were obtained (Pd@NC12-SC12).

Figure 2 presents STEM images, recorded using a HAADF detector (HAADF-STEM), of Pd@NC12 and Pd@SC12 NPs. In this configuration –also called *Z*-contrast imaging– the intensity of the signal is approximately proportional to the square of the atomic number ($\sim Z^2$) of the elements in the specimen and its thickness.[30] Consequently, Pd atoms from the NPs appear with white contrast on the image surrounded by the almost black background corresponding to the amorphous carbon support. As insets in Figure 2, high-resolution HAADF-STEM images of Pd@SC12 and Pd@NC12 are also shown. The results observed in these images disagree with the model proposed by Sun, *et al.*, for Pd@SC12 NPs prepared in a similar way.[31] In that paper, the authors proposed that Pd(0) clusters were immersed in a palladium sulfide phase. If this were the case, the background of the HAADF-STEM images should be brighter than in our micrographs, due to the presence of the Pd atoms surrounding the NPs. Thus, we can affirm that Pd atoms are constrained into a well defined size on the order of ~3 nm, rather than dispersed in an extended palladium sulfide phase.

The high-resolution HAADF-STEM images also show a clear difference in the crystallinity of the particles. While Pd@NC12 NPs present a crystalline structure, it was not possible to distinguish lattice fringes in any of the images of Pd@SC12 NPs for any defocus value. This is clear evidence that the crystal structure of the particle is largely affected by the capping agent: the strong Pd-thiolate interaction or the incorporation of sulfur, as sulfide, on the nanoparticle surface could be responsible for these distortions. Similar results were already obtained, but the physical origin of those images remains unclear.[17,32,33] A detailed study on these phenomena, supported by image simulations, will be reported in a future work.

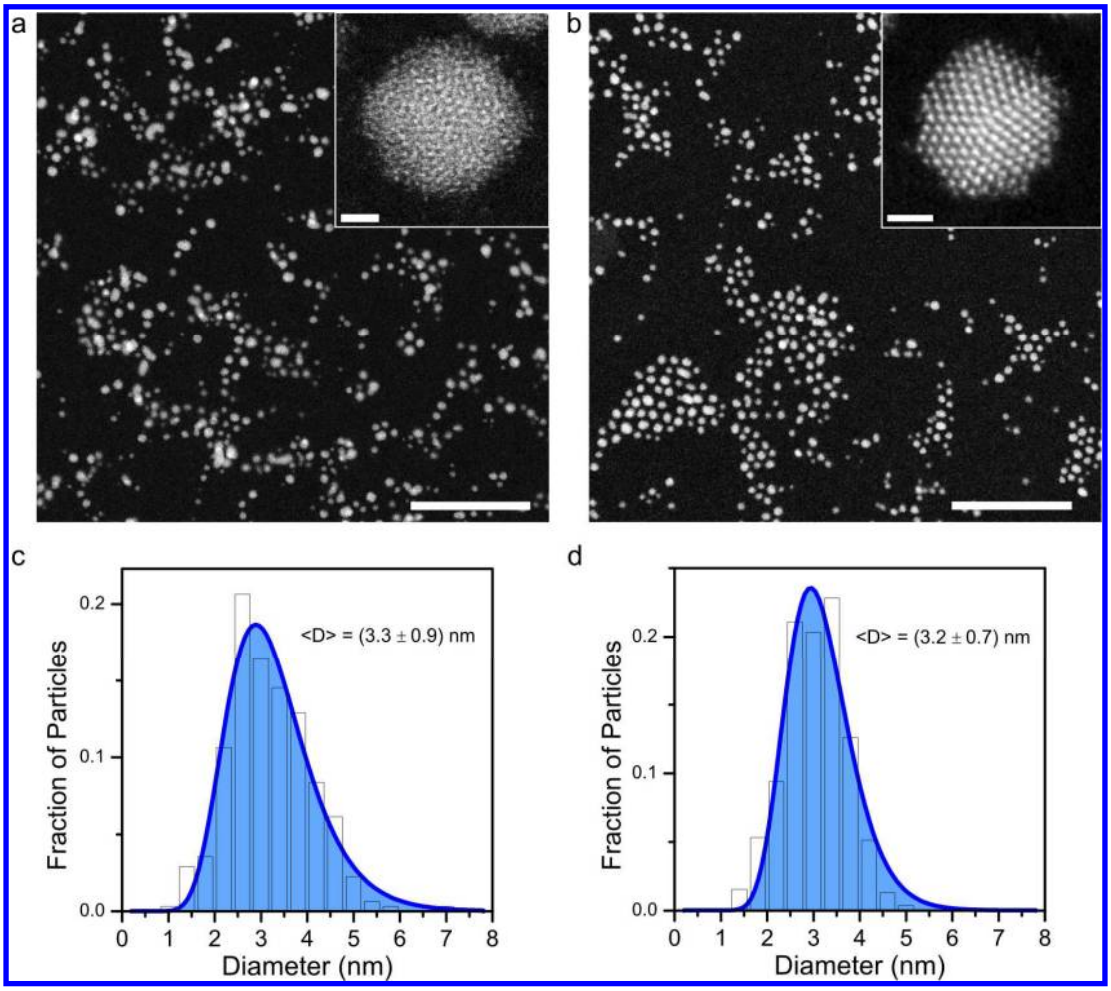

Figure 2. Representative HAADF-STEM images of **a)** Pd@SC12 NPs **b)** Pd@NC12 NPs. Scale bars = 50 nm. The insets show high-resolution images of the NPs (scale bars = 1 nm). Particle size distribution histograms and their Log-normal fit for **c)** Pd@SC12 NPs and **d)** Pd@NC12 NPs.

FTIR spectroscopy was used to verify the presence of the dodecanethiol derived species as protecting agents of the Pd@SC12 NPs. The position of the methylene symmetric (d^+) and antisymmetric (d^-) CH_2 stretching vibrations (ν_{d+}=2850 cm^{-1} and ν_{d-}=2921 cm^{-1}) in the FTIR spectrum (Figure 3) reveals that the alkyl chains are present and extended in a trans zigzag conformation.[34] The absence of an absorption peak in the ν(S–H) region (inset of Figure 3), which appears at 2575 cm^{-1} for free dodecanethiol, indicates the breakage of the S–H bond of the dodecanethiol.[35] In the low wavenumber region of the

spectrum, the peak at 720 cm^{-1} (P_1) is the principal band of the rocking progression.[34] As reported for thiolate-covered Au nanoparticles,[36] the C–S stretches adjacent to trans methylene units $\nu(C–S)_T$ appears as a significantly intense shoulder at 700 cm^{-1}.[36,37] On the other hand, the gauche band $\nu(C–S)_G$ was undetectable (*i.e.*, the uncertainty associated with the background subtraction has a magnitude comparable to the intensity of the small peaks observed for wavenumbers smaller than 700 cm^{-1}). Thus, we can conclude that the number of adsorbates with the C–C bond adjacent to the C–S in gauche conformation is relatively low. Contrary to our results, a 100% gauche conformation, which was interpreted considering dioctyl-disulfide as capping species, was found for octanethiol-protected Pd NPs.[16] See the Supporting Information for a detailed analysis of the FTIR data.

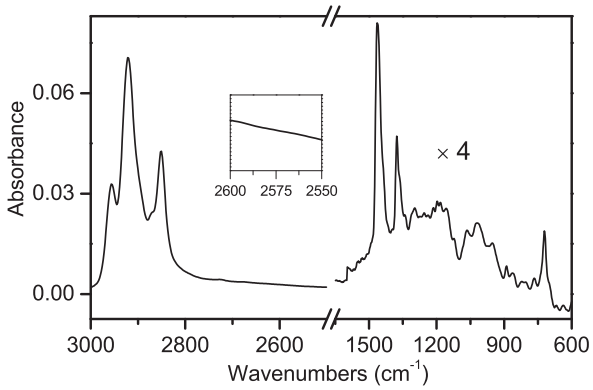

Figure 3. FTIR spectrum of Pd@SC12 NPs. The absorbance in the region between 1650 and 600 cm^{-1} was multiplied by a factor of 4. In the inset, the region near 2575 cm^{-1} is amplified to verify the absence of the peak corresponding to $\nu(S–H)$.

In the following, X-ray absorption and photoelectron spectroscopies will give valuable information with regards to the structure, chemical composition and electronic properties of Pd NPs.

In order to carry out the EXAFS analysis, a dry sample of Pd@SC12 NPs was studied at the Pd K-edge to determine the radial distribution of the atoms, *i.e.*, the average coordination number and Pd-bond distances. EXAFS spectrum of bulk Pd was also recorded for comparison and calibration purposes. The Fourier Transform (FT) of the EXAFS data corresponding to Pd NPs is shown in Figure 4. This

spectrum exhibits two main contributions between 0.13 and 0.28 nm (uncorrected for the photoelectron phase shifts). The presence of Pd–Pd contribution with a bond distance longer than that of the bulk Pd can be determined by comparison with the FT of the Pd foil signal.[19,31,38] We attribute the contribution in the FT between 0.13 and 0.21 nm to the presence of Pd–S coordination shells.[15,19,31,38] To analyze the first nearest neighbor region we did a nonlinear curve fit using the IFEFFIT package,[39,40] integrated into the ATHENA and ARTEMIS user interfaces. The fitted parameters for each coordination shell proposed in the model were the average coordination number (N), path length (d), correction to the threshold energy (ΔE_0) and Debye-Waller factor (σ^2). To perform the fitting, two different shells were proposed, one to take into account the Pd–Pd contribution and the other one corresponds to the Pd–S shell. These contributions were calculated using the FEFF code[41] from crystallographic structure of metallic Pd and palladium sulfide. Since sulfur from the sample suffered from radiation induced damage during the measurements (generation of high oxidation state sulfur species), the deconvolution of this signal into contributions of different Pd–S distances coming from different sulfur species might not be reliable. Accordingly, the Pd–S shell was fitted considering only one species, although it can be composed by different compounds. The results of the analysis of the EXAFS data shown in Figure 4 are reported in Table 1.

The small N value (1.8 ± 0.6) for the Pd–Pd contribution cannot be only explained by the formation of small Pd NPs. Instead of that, another phase with no Pd as first neighbors is needed in order to explain the low N. This is due to the fact that this parameter represents an average over all Pd atoms present in the sample. If a fraction of Pd atoms is forming a structure in which they are bonded to a different type of atom, they will contribute with zero to the Pd–Pd average coordination number. The Pd–Pd distance obtained in the fitting of Pd@SC12 NPs (0.275 ± 0.001 nm) is larger than that obtained for bulk Pd (0.273 ± 0.001 nm). Similar results for Pd–Pd distances in Pd NPs capped with thiols were obtained earlier.[31,38]

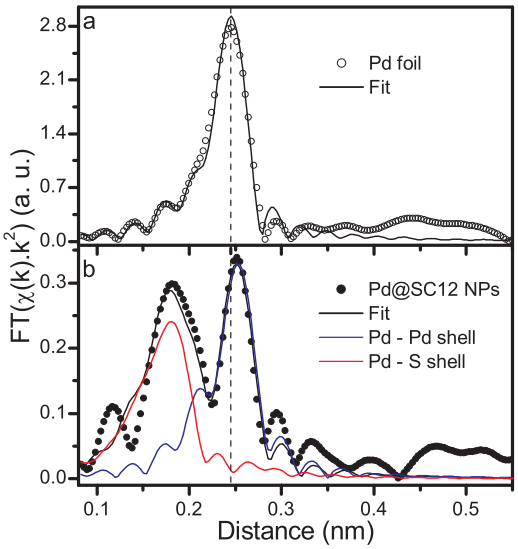

Figure 4: Experimental Fourier Transform and corresponding fits of the EXAFS signal for **a)** Pd foil and **b)** Pd@SC12 NPs sample.

Table 1. Structural parameters of Pd@SC12 NPs obtained by EXAFS.[1]

.	Pd@SC12 NPs		Pd Foil
	Pd–Pd shell	Pd–S shell	Pd–Pd shell
N	1.8 ± 0.6	1.3 ± 0.5	12
ΔE_0 (eV)	7 ± 2	7 ± 2	-1 ± 2
σ^2 (10^{-5} nm^2)	6 ± 2	7 ± 4	4.4 ± 0.6
d (nm)	0.275 ± 0.001	0.229 ± 0.003	0.273 ± 0.001

The EXAFS data agrees with previous studies. However, the low N was interpreted by two models. The first one proposes Pd(0) clusters immersed in a palladium sulfide phase, which we discarded based on our HAADF-STEM analysis.[31] The second one proposes a Pd-core PdS_x-shell structure covered by thiolate moieties, in analogy with the planar Pd surfaces modified with thiols.[19,38] However, the EXAFS

[1] Average coordination number (N), path distance (d), threshold energy correction (ΔE_0) and Debye-Waller exponent (σ^2).

data gave no further details with regards to the chemistry of the S/Pd interface, or the processes that occur during the formation of NPs.

In order to address the surface chemical composition of Pd@SC12 NPs we will discuss XPS data of this material, in relation with results obtained for dodecanethiolate-protected Au NPs (Au@SC12, prepared as explained in the Supporting Information), Pd@NC12, Pd@NC12-SC12 NPs and dodecanethiolate SAMs on extended Pd and Au surfaces.

XPS spectra for the Pd@SC12 NPs show a broad S 2*p* signal at ~162.5 eV (Figure 5a). The analysis of the S 2*p* and Pd 3*d* signals indicate that the total sulfur to palladium ratio (S:Pd = 0.7 ± 0.1) is twice the value found for the S:Au ratio in Au@SC12 NPs of comparable size. On the other hand, the same factor is found in the (S:Pd)/(S:Au) ratio derived from XPS S 2*p* data of alkanethiolate SAMs on Pd(111)[7,8] and Au(111).[2] This value is clear evidence that there is a sulfur excess in the Pd@SC12 NPs surfaces in relation to that expected in systems where the capping species are alkanethiolates. A similar conclusion can be derived from the thermogravimetric analysis reported by Zamborini, *et al.*, who found a bigger organic content than that predicted based on a simple thiolate adsorption model.[24] On the basis of these results we can immediately discard simple thiolate-Pd interface models reported in recent years for this system.[10,12,13]

The fitting of the S 2*p* peak yields two main components at 162.1 eV and 162.9 eV and a small one at 164.1 eV (Figure 5a). The assignment of the components was done following the work by the Whitesides' group for alkanethiolate adlayers on bulk Pd: thiolates (162.9 eV component) are placed on sites of a diluted sulfide layer (162.1 eV component) adsorbed on the nanoparticle surface.[1,7,8] The assignment of the small 164.1 eV component is more complicated and it could correspond to physisorbed disulfide molecules[7] or physisorbed alkanethiols.[42] Note that our results disagree with the data reported for *n*-octadecyl mercaptan-protected Pd NPs prepared by the two-phase method, for which binding energies were found to range from 161.4 to 161.7 eV.[43]

For the sake of comparison, the S 2*p* components for dodecanethiolate-modified extended planar Pd surfaces are presented (Figure 5b). It is evident that the components in the spectra of planar and nanoparticle Pd surfaces are quite similar, and clearly different from that corresponding to Au@SC12 NPs (Figure 5d) and previously reported data for Au(111) surfaces.[2] These results evidence that sulfur species present on both Pd surfaces, planar and 3 nm NPs, are probably of the same nature. If dialkyldisulfides were the main ligands, as previously proposed,[16] the 163-164 eV component should dominate the S 2*p* signal which is clearly not the case in Pd@SC12 NPs (Figure 5a).

The C:S atomic ratio obtained is smaller than that expected for NPs capped only by thiolate moieties, in concordance with the presence of a mixed sulfide/thiolate adlayer (see Supporting Information).

Dodecanethiolate-protected Pd NPs prepared by ligand place-exchange of Pd@NC12 NPs were also studied by XPS. The alkylamines were partially exchanged by dodecanethiol molecules, resulting in particles with a mixed capping agent (Pd@NC12-SC12 NPs), as revealed by XPS, which evidenced some amount of nitrogen after the ligand place-exchange. In Figure 5c, it can be observed that these NPs have a composition very similar to Pd@SC12 NPs, prepared by the two-phase method. The quantitative data is presented in Table 2. Although the total S:Pd molar ratio was lower compared to Pd@SC12 NPs, due to an incomplete exchange of the ligands, the contributions to the S 2*p* peak show the presence of sulfide in these NPs. This makes evident the S–C bond breakage by Pd core upon thiol adsorption. Even though these two routes to obtain thiolate-protected NPs are completely different, the final composition is very similar.

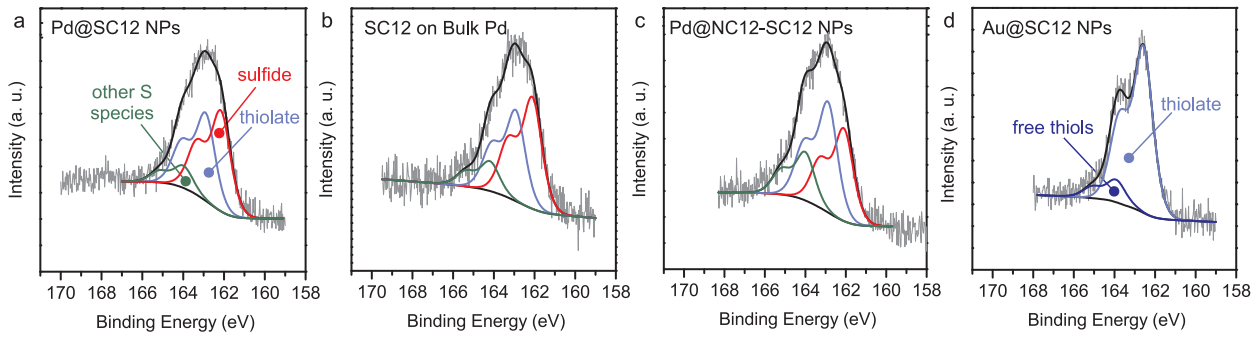

Figure 5. The S 2*p* spectra of different systems are shown for comparison. **a)** Pd@SC12 NPs prepared by two-phase Brust-Schiffrin method, **b)** Dodecanethiol adsorbed on bulk Pd, **c)** Pd@NC12-SC12 NPs prepared by ligand place-exchange of Pd@NC12 NPs with dodecanethiol, **d)** Au@SC12 NPs prepared by two-phase Brust-Schiffrin method.

Table 2. XPS data for different dodecanethiolate-covered Pd surfaces.[2]

	Pd Bulk	**Pd@SC12 NPS**	**Pd@NC12-SC12 NPs**
Sulfide	48 ± 3 %	46 ± 2 %	37 ± 3%
Thiolate	39 ± 4 %	42 ± 3 %	44 ± 4%
-S-S-, S_n or physisorbed thiols	13 ± 2 %	12 ± 3 %	19 ± 6 %

In order to get insight into the distribution of the different sulfur species in the nanoparticles we carried out high resolution XPS measurements with X-rays of lower energies. The 250 eV synchrotron light used for the analysis of the S 2*p* signal produces photoelectrons of markedly lower kinetic energies

[2] Relative contribution of the different components of the S 2*p* signal for dodecanethiol SAM on bulk Pd, Pd NPs prepared by Brust-Schiffrin method (Pd@SC12) and Pd NPs prepared by ligand place-exchange of Pd@NC12 NPs (Pd@NC12-SC12 NPs).

than those produced in our laboratory with Mg Kα source. The measurements at 250 eV allowed sensitivity to the composition of the surface rather than to the whole nanoparticle. In this regard, it is interesting to note that the inelastic mean free path of the S 2*p* photoelectrons emitted due to the incidence Mg Kα radiation (1253.6 eV) in a metallic phase is about 2.5 nm, while for those produced by an incident photon energy of 250 eV it is estimated to be 0.5 nm.[44] The deconvolution of the spectrum taken with 250 eV (see Supporting Information) showed the same thiolate to sulfide area ratio (~ 1) that was found with the Mg Kα source (~ 0.9), within the experimental error. If sulfide were homogeneously distributed in the cores of the Pd@SC12 NPs, its relative contribution to the S 2*p* signal should be smaller in the case 250 eV incident energy. Thus, we can infer that thiolate and sulfide species are both at the surface of the NPs. Based on it, we can discard the idea of sulfide homogeneously distributed in the cores of the nanoparticles.

In summary, independently of the route used to produce thiolate-protected NPs and the nature of the surface (extended planar or NPs), comparable amounts of thiolate and sulfide species are found as components of the systems. Additionally, the sulfur species are located in the surface of the nanoparticles. It is important to note that this last conclusion could not be reached from EXAFS or conventional XPS.

The analysis of the Pd 3*d* signal is also important to understand the nature of sulfur species on Pd nanoparticle surface. When compared to clean Pd surface, the samples prepared in the presence of thiols exhibit a significant shift towards greater binding energies, indicating partial Pd oxidation, which has been related to the presence of PdS_x at the interface.[8,33] However, as it was already stated by Cook, *et al.*[45] the positive BE shift, can be produced by several effects. XPS measurements of supported metal clusters and calculations on core-level binding energy shifts have been reported. In this studies several phenomena have been proposed to explain values up to ~ 1 eV in the binding energy shifts.[46–50]

The study of the valence-band spectra can yield valuable data on the behavior of metals towards the adsorption of different species, since the reactivity of transition metals is closely related to the

population of the *d*-band. The closer the *d*-band center is to the Fermi level, the easier the charge transfer between the metal surface and the adsorbate states. Therefore, metals with *d*-bands populated near the Fermi level are capable of breaking bonds of the adsorbates on their surface. Figure 6 shows the valence-band spectra of Pd@SC12 and Au@SC12 NPs, measured with Mg Kα source. As it is observed, the valence-band of Au NPs is located at greater binding energies than the one of Pd NPs. As already known in catalysis, this fact is closely related to the high reactivity of Pd compared to Au. The changes in the density of states (DOS) of Pd(111) as a consequence of methanethiol adsorption, were recently analyzed by means of density functional theory (DFT).[1] It was proposed that the presence of sulfide species on Pd surfaces in contact with thiol molecules is produced due to the S–C bond rupture by Pd.[1] Upon thiol adsorption on Pd, there is an electron density transfer from the metal *d*-band to the antibonding molecular orbitals of thiol molecules that weakens the S–C bond, resulting in the elongation and finally breakage of S–C bond. It was verified by DFT that after the adsorption of sulfide atoms on Pd(111), the surface is passivated, and the position of the *d*-band is shifted towards values more similar to the ones found on Au, where it is known that S–C bond scission does not occurs for the case of alkanethiols. Once some sulfide is adsorbed, the surface cannot break more S–C bonds and, accordingly, the thiols adsorption becomes possible on top of this diluted palladium sulfide layer. Cook, *et al.*,[45] attributed a valence-band shift to a higher *d*-electron depletion on thiolate-protected Pd NPs compared to alkylamines-protected particles. This *d*-electron depletion is produced by the charge transfer from Pd to adsorbed sulfur species.

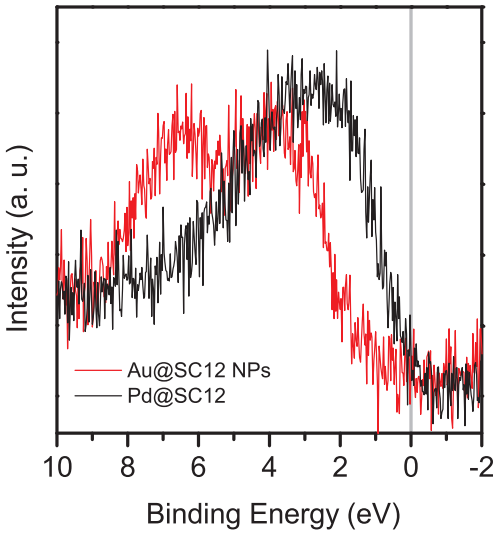

Figure 6. Valence band signal for Pd@SC12 NPs compared with Au@SC12 NPs. The intensity was normalized by the intensity of Pd 3*d* and Au 4*f* signal, respectively.

Based on the analysis of the above presented experimental data and the DFT results previously published, we present a plausible explanation for the processes that occur during the synthesis of dodecanethiolate-protected Pd NPs. In the case of place-exchange of dodecylamine by dodecanethiol, the processes should be very similar to the ones observed on extended planar Pd surfaces. Thiol molecules might replace alkyl amine molecules and approach the metallic Pd, which is able to cleave the S–C bond, and produce sulfide adsorbates. At this point, the particle surface is not active anymore for the alkanethiol decomposition into sulfide, but it is able to adsorb dodecanethiolate moieties. Thus, the depletion of the population of valence-band electrons near the Fermi level explains why the Pd NPs are not completely sulfidized. Since Pd@NC12-SC12 NPs, prepared through the ligand-exchange strategy, showed the same sulfur species than those prepared following the two-phase Brust-Schiffrin method, it is reasonable to propose a similar mechanism for the final steps in the formation of Pd@SC12 NPs. This method starts with the addition of alkanethiol to the organic phase, which partially converts the Pd(II) halogenide complexes into Pd(II)-thiolate complexes. Upon addition of the reducing agent, Pd(0) nuclei are formed. The small metallic particles grow in the presence of several species that can be adsorbed on

its surface (tetraoctylammonium cations, halogenides, palladium thiolates, dodecanethiol or species that are related with this thiol). Then, dodecanethiolate-related species might reach the metallic clusters which are able to cleave the S–C bond, and from this point the reaction should continue in the same way than in the other route. However, the synthesis does only drive to stable nanoparticle products if Pd(II) is in stochiometric excess with respect to the thiols (see UV-vis data in the Supporting Information and the results by Zamborini, *et al*.[24]). Nevertheless, further studies are needed to completely elucidate each of the steps in the synthesis of thiolate-protected Pd NPs through the Brust-Schiffrin method, as the ones recently published for the case of Au, Ag and Cu.[25,26,51]

4. CONCLUSIONS

Even today, the chemistry of the thiolate-protected Pd nanoparticles produced either by the two-phase Brust-Schiffrin method or by the ligand place-exchange method is not well understood. Based on diverse experimental results, they have been described by different groups in terms of simple thiolate-capped Pd(0) particles –similar to thiolate-capped Au NPs–, alkyldisulfide-capped Pd(0) particles, palladium sulfide particles, Pd(0) clusters immersed in a palladium sulfide phase or complex thiolate-sulfide capped Pd(0) particles, in analogy to the surface structure reported for alkanethiolate SAMs on Pd(111). Our experimental data for ~ 3 nm diameter Pd NPs prepared by both synthetic routes are consistent with the thiolate-sulfide capped Pd(0) particle composition. The NPs consist of a central core composed of metallic Pd, surrounded by a sulfidized Pd layer to which thiolate ligands are coordinated. Indeed, sulfur species in the Pd NPs should be present at the submonolayer level. In the present work we unambiguously demonstrate that the chemical nature of these particles is very similar to that experimentally found for alkanethiolate-covered bulk Pd and that recently proposed for Pd(111) surface, from DFT models.

The Pd(0) clusters, formed as a consequence of the reduction of Pd(II) species, are likely responsible for the S–C bond cleavage that leads to adsorbed sulfide. The Pd cores modified by submonolayer of sulfide are active for the adsorption of thiolate moieties, but they are not able to further decompose the thiol molecules. This result rules out the complete sulfidization of the Pd NPs, at least at this particle size. Then, the results from this paper are valuable not only for handling thiolate-protected Pd NPs for different applications but also for the basic comprehension of metallic nanoparticles and the relation of their surface structure whit the synthesis method.

Acknowledgment: We thank S. Mejía-Rosales, M. Mariscal and A. Ponce for useful discussions. We acknowledge financial support from Agencia Nacional de Promoción Científica y Tecnológica (PICT 2010-0423, PICT 2006-621, PICT 2010-2554, Nanotechnology Network PAE22711), CONICET (PIP 11220090100139), Universidad Nacional de La Plata, Argentina, Laboratório Nacional do Luz Síncrotron (LNLS), Campinas, Brazil (Research Proposal SGM-11769), The Welch Foundation Agency (project AX-1615: *Controlling the Shape and Particles Using Wet Chemistry Methods and Its Application to Synthesis of Hollow Bimetallic Nanostructures*), the National Science Foundation (NSF) (PREM grant number: DMR-0934218, NSF Grant 1103730: *Alloys at the Nanoscale; The Case of Nanoparticles Second Phase*). G. Corthey gratefully acknowledges the Swiss National Science Foundation (SNSF) and Universidad Nacional de La Plata for financial support.

Supporting Information Available: Synthesis of Pd and Au NPs, UV/Vis study of the different steps in the synthesis of Pd@SC12 NPs, TEM of Au@SC12 NPs, FTIR details, S 2*p* XPS signal of Pd@SC12 NPs acquired with synchrotron radiation. This material is available free of charge *via* the Internet at http://pubs.acs.org.

REFERENCES

1. Carro, P.; Corthey, G.; Rubert, A. A.; Benitez, G. A.; Fonticelli, M. H.; Salvarezza, R. C. *Langmuir* **2010**, *26*, 14655–14662.

2. Vericat, C.; Vela, M. E.; Benitez, G.; Carro, P.; Salvarezza, R. C. *Chem. Soc. Rev.* **2010**, *39*, 1805–1834.

3. Brust, M.; Walker, M.; Bethell, D.; Schiffrin, D. J.; Whyman, R. *J. Chem. Soc., Chem. Commun.* **1994**, 801–802.

4. Bourg, M.-C.; Badia, A.; Lennox, R. B. *J. Phys. Chem. B* **2000**, *104*, 6562–6567.

5. Jadzinsky, P. D.; Calero, G.; Ackerson, C. J.; Bushnell, D. A.; Kornberg, R. D. *Science* **2007**, *318*, 430–433.

6. Templeton, A. C.; Wuelfing, W. P.; Murray, R. W. *Acc. Chem. Res.* **2000**, *33*, 27–36.

7. Love, J. C.; Wolfe, D. B.; Haasch, R.; Chabinyc, M. L.; Paul, K. E.; Whitesides, G. M.; Nuzzo, R. G. *J. Am. Chem. Soc.* **2003**, *125*, 2597–2609.

8. Corthey, G.; Rubert, A. A.; Benitez, G. A.; Fonticelli, M. H.; Salvarezza, R. C. *J. Phys. Chem. C* **2009**, *113*, 6735–6742.

9. Marshall, S. T.; Schwartz, D. K.; Medlin, J. W. *Langmuir* **2011**, *27*, 6731–6737.

10. Marshall, S. T.; O'Brien, M.; Oetter, B.; Corpuz, A.; Richards, R. M.; Schwartz, D. K.; Medlin, J. W. *Nat. Mat.* **2010**, *9*, 853–858.

11. Majumder, C. *Langmuir* **2008**, *24*, 10838–10842.

12. Moreno, M.; Ibañez, F. J.; Jasinski, J. B.; Zamborini, F. P. *J. Am. Chem. Soc.* **2011**, *133*, 4389–4397.

13. Sadeghmoghaddam, E.; Lam, C.; Choi, D.; Shon, Y.-S. *J. Mater. Chem.* **2010**, *21*, 307–312.

14. Novakova, E. K.; McLaughlin, L.; Burch, R.; Crawford, P.; Griffin, K.; Hardacre, C.; Hu, P.; Rooney, D. W. *J. Catal.* **2007**, *249*, 93–101.

15. Ramallo-López, J. M.; Giovanetti, L.; Craievich, A. F.; Vicentin, F. C.; Marín-Almazo, M.; José-Yacaman, M.; Requejo, F. G. *Phys. B* **2007**, *389*, 150–154.

16. Zelakiewicz, B. S.; Lica, G. C.; Deacon, M. L.; Tong, Y. *J. Am. Chem. Soc.* **2004**, *126*, 10053–10058.

17. Cargnello, M.; Wieder, N. L.; Canton, P.; Montini, T.; Giambastiani, G.; Benedetti, A.; Gorte, R. J.; Fornasiero, P. *Chem. Mater.* **2011**, *23*, 3961–3969.

18. Lu, C.-H.; Chang, F.-C. *ACS Catal.* **2011**, *1*, 481–488.

19. Litrán, R.; Sampedro, B.; Rojas, T. C.; Multigner, M.; Sánchez-López, J. C.; Crespo, P.; López-Cartes, C.; García, M. A.; Hernando, A.; Fernández, A. *Phys. Rev. B* **2006**, *73*, 054404.

20. Walter, M.; Akola, J.; Lopez-Acevedo, O.; Jadzinsky, P. D.; Calero, G.; Ackerson, C. J.; Whetten, R. L.; Grönbeck, H.; Häkkinen, H. *Proc. Natl. Acad. Sci. U. S. A.* **2008**, *105*, 9157–9162.

21. Leff, D. V.; Brandt, L.; Heath, J. R. *Langmuir* **1996**, *12*, 4723–4730.

22. Yeh, J. J.; Lindau, I. *At. Data Nucl. Data Tables* **1985**, *32*, 1–155.

23. Chen, S.; Huang, K.; Stearns, J. A. *Chem. Mater.* **2000**, *12*, 540–547.

24. Zamborini, F. P.; Gross, S. M.; Murray, R. W. *Langmuir* **2001**, *17*, 481–488.

25. Li, Y.; Zaluzhna, O.; Xu, B.; Gao, Y.; Modest, J. M.; Tong, Y. J. *J. Am. Chem. Soc.* **2011**, *133*, 2092–2095.

26. Goulet, P. J. G.; Lennox, R. B. *J. Am. Chem. Soc.* **2010**, *132*, 9582–9584.

27. Yang, Z.; Klabunde, K. J.; Sorensen, C. M. *J. Phys. Chem. C* **2007**, *111*, 18143–18147.

28. Yang, Z.; Smetana, A. B.; Sorensen, C. M.; Klabunde, K. J. *Inorg. Chem.* **2007**, *46*, 2427–2431.

29. Ibanez, F. J.; Zamborini, F. P. *J. Am. Chem. Soc.* **2008**, *130*, 622–633.

30. Varela, M.; Lupini, A. R.; Benthem, K. van; Borisevich, A. Y.; Chisholm, M. F.; Shibata, N.; Abe, E.; Pennycook, S. J. *Annu. Rev. Mater. Res.* **2005**, *35*, 539–569.

31. Sun, Y.; Frenkel, A. I.; Isseroff, R.; Shonbrun, C.; Forman, M.; Shin, K.; Koga, T.; White, H.; Zhang, L.; Zhu, Y. *et al. Langmuir* **2006**, *22*, 807–816.

32. Liu, Y.; Wang, C.; Wei, Y.; Zhu, L.; Li, D.; Jiang, J. S.; Markovic, N. M.; Stamenkovic, V. R.; Sun, S. *Nano Lett.* **2011**, *11*, 1614–1617.

33. Lu, W.; Wang, B.; Wang, K.; Wang, X.; Hou, J. G. *Langmuir* **2003**, *19*, 5887–5891.

34. Hostetler, M. J.; Stokes, J. J.; Murray, R. W. *Langmuir* **1996**, *12*, 3604–3612.

35. Manna, A.; Imae, T.; Yogo, T.; Aoi, K.; Okazaki, M. *J. Colloid Interface Sci.* **2002**, *256*, 297–303.

36. Schaaff, T. G.; Shafigullin, M. N.; Khoury, J. T.; Vezmar, I.; Whetten, R. L. *J. Phys. Chem. B* **2001**, *105*, 8785–8796.

37. Hayashi, M.; Shiro, Y.; Murata, H. *Bull. Chem. Soc. Jpn.* **1966**, *39*, 112–117.

38. Murayama, H.; Ichikuni, N.; Negishi, Y.; Nagata, T.; Tsukuda, T. *Chem. Phys. Lett.* **2003**, *376*, 26–32.

39. Newville, M. *J. Synchrotron Rad.* **2001**, *8*, 322–324.

40. Ravel, B.; Newville, M. *J. Synchrotron Rad.* **2005**, *12*, 537–541.

41. Ankudinov, A. L.; Ravel, B.; Rehr, J. J.; Conradson, S. D. *Phys. Rev. B* **1998**, *58*, 7565–7576.

42. Zhong, C.-J.; Brush, R. C.; Anderegg, J.; Porter, M. D. *Langmuir* **1999**, *15*, 518–525.

43. Shen, C. M.; Su, Y. K.; Yang, H. T.; Yang, T. Z.; Gao, H. J. *Chem. Phys. Lett.* **2003**, *373*, 39–45.

44. Powel, C. J.; Jablonsky, A. *NIST Electron Inelastic-Mean-Free-Path Database, Version 1.2, SRD 71*; National Institute of Standars and Technology: Gaithersburg, MD, 2010.

45. Cook, S. C.; Padmos, J. D.; Zhang, P. *J. Chem. Phys.* **2008**, *128*, 154705–11.

46. Wertheim, G. K.; DiCenzo, S. B.; Buchanan, D. N. E. *Phys. Rev. B* **1986**, *33*, 5384–5390.

47. Wertheim, G. K.; DiCenzo, S. B. *Phys. Rev. B* **1988**, *37*, 844–847.

48. Mason, M. G. *Phys. Rev. B* **1983**, *27*, 748–762.

49. Richter, B.; Kuhlenbeck, H.; Freund, H.-J.; Bagus, P. S. *Phys. Rev. Lett.* **2004**, *93*, 026805.

50. Moriarty, P. *Phys. Rev. Lett.* **2004**, *92*.

51. Li, Y.; Zaluzhna, O.; Tong, Y. J. *Langmuir* **2011**, *27*, 7366–7370.

SYNOPSIS TOC